Disorder-mediated enhancement of fiber numerical aperture

Youngwoon Choi,[1,†] Changhyeong Yoon,[1,†] Moonseok Kim,[1] Juhee Yang,[2] and Wonshik Choi[1,*]

[1]*Department of Physics, Korea University, Seoul 136-701, South Korea*

[2]*RSS Center, Korea Electrotechnology Research Institute, Seoul 121-835, South Korea*

**Corresponding author: wonshik@korea.ac.kr*

Received April 25, 2013; revised May 22, 2013; accepted May 27, 2013;
posted May 31, 2013 (Doc. ID 189529); published June 24, 2013

The numerical aperture (NA) of a multimode optical fiber sets the limit of the information transport capacity along the spatial degree of freedom. In this Letter, we report that the application of a highly disordered medium can overcome the capacity limit set by the fiber NA. Specifically, we coated the input surface of a multimode fiber with a disordered medium made of ZnO nanoparticles and transported a wide-field image through the fiber with a spatial resolution beyond the diffraction limit given by the fiber NA. This was made possible because multiple scatterings induced by the disordered medium physically increased the NA of the entire system. Our study will lead to enhancing the spatial resolution of fiber-based endoscopic imaging and also improving the information transport capacity in optical communications. © 2013 Optical Society of America

OCIS codes: (110.3175) Interferometric imaging; (110.0113) Imaging through turbid media; (110.2350) Fiber optics imaging.

http://dx.doi.org/10.1364/OL.38.002253

Optical fibers have been serving as the backbone of signal transmission in optical communications, and also widely used for image delivery in medical practices. In order to transport information through a fiber, the temporal degree of freedom was mainly used at the initial stage of technology development in conjunction with the use of a single-mode optical fiber. Much effort has been made to exploit spatial degree of freedom as well to boost the data transfer rate [1]. Multimode optical fibers, instead, were used for this purpose and information was delivered through multiple spatial modes called LP modes. Examples include image reconstruction by circular spatial distribution of a fiber [2], image transport through a single fiber by spectral encoding [3] and phase conjugation [4,5]. Advances have been made in recent years to realize endoscopic imaging through a single multimode optical fiber [6–9]. The main idea was to shape an incident wave entering the fiber such that a focused spot was generated at the opposite side of the fiber. Proper change of the incident wave provided scanning of the focused spot. Our group also demonstrated wide-field endoscopic imaging operated in a reflection mode [10]. In that study, we recorded a transmission matrix of a single multimode fiber, which characterized output field responses to various input modes, and applied the inversion of the transmission matrix to eliminate the effect of image distortion by the fiber [10]. Later, we made use of a transmission matrix for determining spatial mode properties of an arbitrarily shaped fiber [11]. However, in all the preceding studies where spatial degree of freedom was used, the numerical aperture (NA) of fibers imposed a fundamental limit on the bandwidth of spatial frequency. We noted that a highly scattering medium can physically extend the NA of an imaging system [12], because multiple scatterings caused by the scattering medium can convert high spatial frequency inputs into low spatial frequency components.

In this Letter, we propose a method that uses a disordered medium to enlarge the spatial passband of a multimode fiber beyond the limit determined by the fiber NA. In order to experimentally prove the proposed concept, we demonstrated that a wide-field image with a spatial resolution surpassing the diffraction limit set by the fiber NA can be transported through a multimode optical fiber. Specifically, ZnO nanoparticles were randomly deposited on the input surface of a multimode fiber and the transmission matrix of the random-material-coated fiber was measured. Object information was then sent through the fiber and the image distortion was reversed by the recently developed turbid lens imaging technique [12].

The experimental setup is depicted in Fig. 1(a). Light waves emitted from a He–Ne laser ($\lambda = 633$ nm) were split into a sample beam and a reference beam by a beam splitter (BS1). The sample beam was delivered to the input surface of a fiber at the object plane (OP) via a two-axis galvanometer mirror (GM), a spatial light modulator (SLM: Hamamatsu Photonics, X10468-06), and a 4-f telescope composed of an objective lens (OL_T: Olympus, ACHN20XP; 20×) and a tube lens. After being injected into the fiber at the OP, the sample beam was guided and delivered to the opposite surface of the fiber located at the image plane (IP). The output wave was collected by an OL (Olympus, ACHN40XP; 40×) and delivered to a CMOS camera (RedLake, M3; 500 fps) via a tube lens, a 4-f telescope, and a beam splitter (BS2). The SLM positioned at the plane conjugated to the OP worked as a normal mirror when a flat pattern was written, and served as a test object when a target pattern was loaded. The reference beam was combined with the sample beam at BS2 to form an interference image at the camera. The polarization of the output wave was set the same as that of the reference beam for the maximum interference contrast. An electric field image was extracted from the interference image by using the digital holographic technique [13]. In this experiment, we prepared two 1 m long multimode optical fibers (Thorlabs, M14L01; 0.22 NA) with a core diameter of 50 μm and a clad thickness of 37.5 μm. One of the fibers was left intact as a reference, whereas for the other, a disordered medium was coated on the input surface at OP by spraying ZnO nanoparticles.

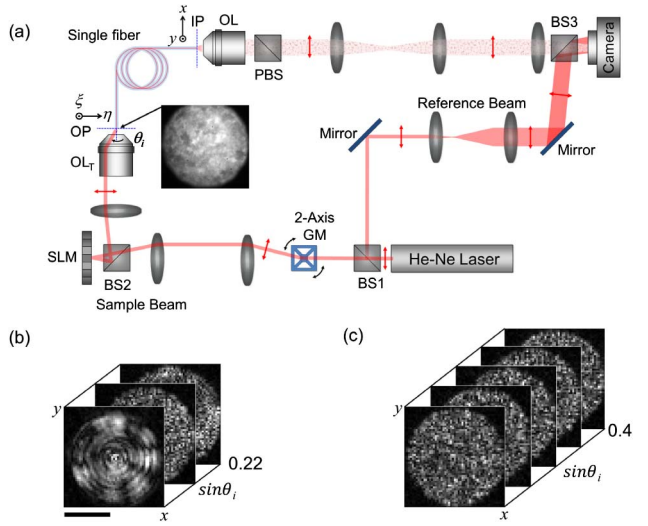

Fig. 1. (a) Schematic diagram of the experimental setup. BSi, i-th beam splitter; PBS, polarizing beam splitter; GM, galvanometer mirror; OP, object plane; IP, image plane; OL and OL$_T$, objective lenses. The red arrows indicate the direction of polarization. The photograph next to the OL$_T$ shows the bright-field image of the input surface of the fiber coated by nanoparticles. (b), (c) Representative measured output images as a function of the incident angle ($\sin\theta_i$) of plane waves at OP, for the intact fiber (b) and the nanoparticle-coated fiber (c), respectively. Scale bar, 25 μm.

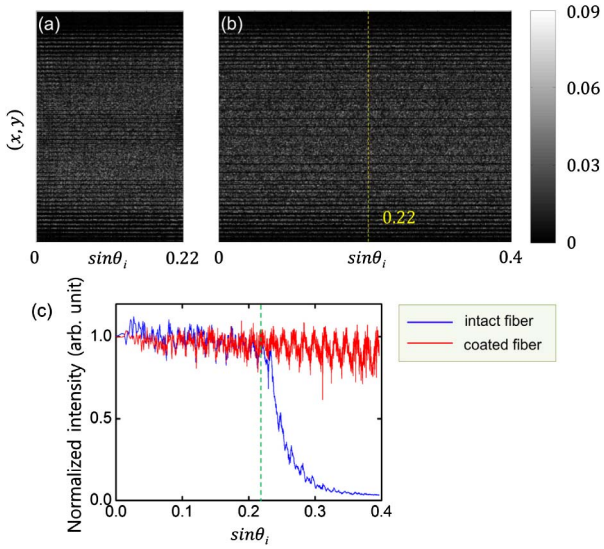

Fig. 2. (a) Measured transmission matrix of the intact fiber. The matrix elements were acquired up to the fiber NA. (b) Measured transmission matrix of the random fiber. The measurable input range was extended over the fiber NA (yellow dashed line). Vertical and horizontal indices represent the position at IP and input angle θ_i at OP, respectively. Color bar: arbitrary intensity unit. (c) Average intensity of the column of the transmission matrix as a function of incident angle. The intensity was normalized with respect to that of $\theta_i = 0$. The dashed line denotes the fiber NA.

Relative transmittance of the coated fiber was 0.5% to that of the intact fiber.

In order to record a transmission matrix, T, of the fiber, the sample beam was steered by the GM such that the input angle, θ_i, was scanned at the OP with a uniform angular sampling density. For the intact fiber, 2000 images were taken for the transmission matrix, whose angular scanning range corresponded to $NA_{tr} = 0.22$, exactly the same as the fiber NA. When the incident angle was beyond this value, light transmission was significantly attenuated. Some representative transmission images are shown in Fig. 1(b). With the nanoparticle-coated fiber, however, light transmission at incident angles larger than the fiber NA was maintained at a similar level to that of the smaller incident angles. For the coated fiber, we measured the transmission matrix up to $NA_{tr} = 0.4$, 1.8 times larger than the maximum NA of the fiber. We recorded 5000 images in 10 s. Some representative transmission images are presented in Fig. 1(c). The plane wave inputs were completely distorted by the random material and by the mode mixing of the fiber.

With the recorded images, the transmission matrix, T, was constructed by converting each two-dimensional image into a single vector and appending it in a column in a sequential way [11,14]. For the intact fiber, the measured T is shown in Fig. 2(a). The average intensity of each column vector in T is plotted as a function of input angle θ_i in Fig. 2(c). The transmitted intensity retains almost the same value up to 0.22 NA, but decreases sharply beyond this point due to the limited NA of the fiber. For the coated fiber, on the other hand, T is significantly large well beyond the fiber NA [Fig. 2(b)] and the average intensity stays almost in the same range, as shown in Fig. 2(c). This is because multiple scatterings induced by the nanoparticles at the input surface fold the input waves outside the fiber NA into the passband. In other words, the disordered medium extends the acceptance angle of the fiber [12]. Therefore, one can expect that the extension of the transmission matrix leads to enlargement of the fiber passband for information delivery.

After measuring the transmission matrix, a test object was loaded on the SLM. The object consisted of stripe patterns similar to a United States Air Force (USAF) target with various widths and lengths (Fig. 3). The peak-to-peak distances of line pairs indicated by numbers 2, 3, and 4 were 1.8, 1.5, and 1.2 μm, respectively, at the OP. After the target image was transported through the fiber, the distorted object image at the IP, $E_{IP}(x, y)$, was taken by the camera. One thousand object images were recorded while scanning the illumination beam onto the test object up to the maximum angle corresponding to the fiber NA, 0.22, at OP. Therefore, the NA for the illumination, NA_{ill}, was set as 0.22. From each distorted image at the IP, we reconstructed the object image at the OP by multiplying the inversion matrix of the measured T [10,12]:

$$E_{OP}(\xi, \eta) = T^{-1} E_{IP}(x, y). \quad (1)$$

Here, $E_{OP}(\xi, \eta)$ is the object image at the OP and T^{-1} represents the inverse of the transmission matrix. Using Eq. (1), the distortion imposed by the fiber itself (for the intact fiber) or by the fiber and the nanoparticles (for the coated fiber) can be eliminated. The Matlab built-in function *pinv* was used for the inversion operation. After the process, all reconstructed images were incoherently added to produce the final objective image.

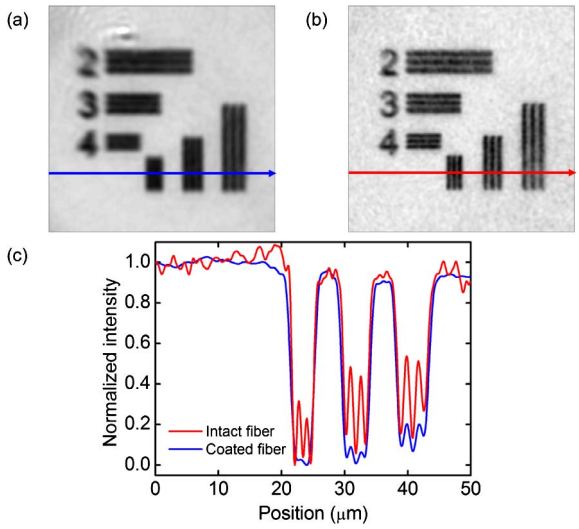

Fig. 3. (a) Reconstructed image transported through the intact fiber. The smallest structures in group 4 are blurred due to the lack of resolving power. (b) Reconstructed image from the output through the nanoparticle-coated fiber. The structural details in group 4 can be resolved. Scale bar: 10 μm. (c) Section profiles along the lines shown in (a) and (b). The improved resolution is verified by the comparison of the two section profiles.

For the case of the intact fiber, the reconstructed object image is shown in Fig. 3(a). In this case, the NA of the measured transmission matrix, $NA_{tr} = 0.22$, and the NA of the illumination, $NA_{ill} = 0.22$, set the diffraction limit as $1.22\lambda/(NA_{tr} + NA_{ill}) = 1.8$ μm. As a result, the patterns in groups 3 and 4 are not resolved. In other words, the transmission of high spatial frequency information forming the stripes in groups 3 and 4 through the fiber is forbidden. In contrast to the case of the intact fiber, the stripes in group 3 are clearly resolved when the nanoparticle-coated fiber was used [Fig. 3(b)], because the increased NA of the transmission matrix ($NA_{tr} = 0.4$) with the same $NA_{ill} = 0.22$ increases the achievable resolution limit up to 1.25 μm. This allows the spatial frequency band, that used to be forbidden, to open through the fiber and consequently more information can be delivered through the newly released passband. The finest stripes in group 4 are barely, but still resolved since the achievable resolution is almost the same as the peak-to-peak distance of the structure. Figure 3(c) presents section profiles for both images. This confirms that the resolving power is considerably improved by employing a highly disordered medium on the input surface of a multimode fiber. In return, the SNR of the reconstructed image was somewhat decreased with the use of the disordered medium.

In conclusion, we have experimentally demonstrated that the spatial passband of a multimode optical fiber can be extended beyond the limit imposed by the fiber NA. By depositing nanoparticles on the input surface of a multimode fiber in a random fashion, transmission properties of the fiber were modified. Particularly, the acceptance angle of the fiber was significantly increased due to the multiple scatterings induced by the nanoparticle layer. By using the transmission matrix of the coated fiber, high spatial frequency inputs embedded in the distorted output images were faithfully reconstructed and, consequently, a wide-field image was successfully delivered through the multimode fiber with improved spatial resolution mediated by the disordered medium. Our study will lay a foundation for the application of disordered media to improve the spatial resolution of fiber-based endoscopic imaging and enhance the information transport capacity in optical communications beyond the limit imposed by the fiber NA. As a final remark, wide range of various materials such as microlenses that can manipulate the angle of incident wave can be used in our method to obtain the similar enhancement of fiber NA.

This research was supported by the Basic Science Research Program through the National Research Foundation of Korea funded by the Ministry of Education, Science and Technology (2010-0011286 and 2011-0016568), the National R&D Program for Cancer Control, the Ministry of Health & Welfare, South Korea (1120290), the Seoul Metropolitan Government, Korea under contract of R&BD Program WR100001.

†Equally contributed.

References

1. H. R. Stuart, Science **289**, 281 (2000).
2. A. A. Friesem and U. Levy, Opt. Lett. **2**, 133 (1978).
3. A. L. Aan de Kerk, Int. Ophthalmol. **3**, 191 (1981).
4. B. F. a. S. Sternklar, Appl. Phys. Lett. **46**, 113 (1985).
5. J. Y. Son, V. I. Bobrinev, H. W. Jeon, Y. H. Cho, and Y. S. Eom, Appl. Opt. **35**, 273 (1996).
6. S. Bianchi and R. Di Leonardo, Lab Chip **12**, 635 (2012).
7. T. Cizmar and K. Dholakia, Nat. Commun. **3**, 1027 (2012).
8. R. N. Mahalati, R. Y. Gu, and J. M. Kahn, Opt. Express **21**, 1656 (2013).
9. I. N. Papadopoulos, S. Farahi, C. Moser, and D. Psaltis, Biomed. Opt. Express **4**, 260 (2013).
10. Y. Choi, C. Yoon, M. Kim, T. D. Yang, C. Fang-Yen, R. R. Dasari, K. J. Lee, and W. Choi, Phys. Rev. Lett. **109**, 203901 (2012).
11. C. Yoon, Y. Choi, M. Kim, J. Moon, and W. Choi, Opt. Lett. **37**, 4558 (2012).
12. Y. Choi, T. D. Yang, C. Fang-Yen, P. Kang, K. J. Lee, R. R. Dasari, M. S. Feld, and W. Choi, Phys. Rev. Lett. **107**, 023902 (2011).
13. T. Ikeda, G. Popescu, R. R. Dasari, and M. S. Feld, Opt. Lett. **30**, 1165 (2005).
14. M. Kim, Y. Choi, C. Yoon, W. Choi, J. Kim, Q.-H. Park, and W. Choi, Nat. Photonics **6**, 581 (2012).